(Red color indicating the main revisions)

Co-seismic surface ruptures produced by the 2014 M_w 6.2 Nagano earthquake, along the Itoigawa–Shizuoka Tectonic Line, central Japan

Aiming Lin[1*], Mikako Sano[1], Bing Yan[1,2], and Maomao Wang[1]

[1]Department of Geophysics, Graduate School of Science
Kyoto University, Kyoto 606-8502, Japan

[2]Graduate School of Science and Technology, Shizuoka University,
Ohya 836, Shizuoka 422-8529, Japan

****

***Corresponding author**
Dr. Aiming Lin
Department of Geophysics
Graduate School of Science
Kyoto University
Kyoto 606-8502, Japan
Email: slin@kugi.kyoto-u.ac.jp

Abstract

Field investigations reveal that the Mj 6.8 (M_w 6.2) Nagano (Japan) earthquake of 22 November 2014 produced a 9.3-km-long co-seismic surface rupture zone. Slip occurred on the pre-existing active Kamishiro Fault, which is developed along the Itoigawa–Shizuoka Tectonic Line, which is inferred as the boundary between the Eurasian and North American plates. The surface-rupturing earthquake produced dominant thrusting and subordinate strike-slip displacement. Structures that developed during the co-seismic surface rupture include thrust faults, fault scarps, *en-echelon* tension cracks, folding structures such as mole tracks and flexural folds, and sand-boils. The surface displacements measured in the field range from several centimeters to 1.5 m in the vertical (typically 0.4–1 m), accompanied by a strike-slip component that reached 0.6 m along NNE-trending ruptures. These observations indicate a thrust-dominated displacement along the seismogenic fault. Our results show that (i) the pre-existing Kamishiro Fault, which strikes NNE–SSW, controlled the spatial distribution of co-seismic surface ruptures and displacements; and (ii) the style and magnitude of thrust displacements indicate that the present-day shortening strain on the Eurasian–North American plate boundary in the study area is released mainly by seismic thrust displacements along the active Kamishiro Fault.

Keywords: 2014 M_w 6.2 Nagano earthquake, co-seismic surface rupture, Kamishiro Fault, Itoigawa–Shizuoka Tectonic Line, plate boundary, thrust

1. Introduction

The 2014 M_w 6.2 (Mj 6.8) Nagano earthquake occurred at 22:08 (Japan Standard Time) on 22 November, 2014 and resulted in extensive damage in the intermontane area of northern Nagano Prefecture, central Japan (Fig. 1; Japan Meteorological Agency, 2014). A maximum seismic intensity of 6.0-Lower (on the Japanese seven-point seismic intensity scale) was observed in the area around the epicenter of the earthquake. Our survey group traveled to the epicentral area one day after the earthquake to investigate the mechanism, earthquake surface deformation features, and nature of the seismogenic fault. We undertook one week of fieldwork, during which time we collected primary field data related to the geometry, morphology, and spatial distribution of co-seismic surface displacements. One week after the earthquake, the study area was covered by heavy snow. Recently, we carried out additional field investigations for 3 days after thawing five months after the earthquake. Here, we report the main results of our field investigations. We also discuss the co-seismic rupturing mechanism and the implications of our findings for the seismo-tectonics of the Itoigawa–Shizuoka Tectonic Line (ISTL) within our study are (Fig. 1a).

2. Tectonic setting

The study region is located in the Matsumoto and Kamishiro basins of northern Nagano Prefecture in Honshu Island, Japan, where the ISTL is inferred as the boundary between the Eurasian and North American plates (Fig. 1a) (e.g., Kobayashi, 1983; Nakamura, 1983; Seno et al., 1993, 1996). The ISTL generally strikes NNE-SSW to NNW-SSE and extends for

62 ~150 km long (Fig. 1a). South of the study area, the ISTL in southern Honshu Island forms
63 one arm of the triple junction of the Eurasian, North American, and Philippine Sea plates.
64 Previous studies have shown that the ISTL is one of the most important active fault zones in
65 central Japan (Fig. 1a) (Research Group for Active Faults of Japan [RGAFJ], 1980, 1991)
66 and that it represents a geological boundary that divides Honshu Island into western and
67 eastern provinces (Geological Society of Japan, 2006). The Kamishiro Fault is a major active
68 section of the ISTL Fault System that dips at 30°–70° to the east. It strikes generally N–S to
69 NNE–SSW along a length of ~26 km, forming the northern boundary that separates the
70 Matsumoto and Kamishiro basins in the west, from the Saigawa Hills in the east (Fig. 1b;
71 RGAFJ, 1980, 1991; Headquarters for Earthquake Research Promotion, 2014). Basement
72 rocks on the western side of the Matsumoto and Kamishiro basins consist mainly of
73 pre-Neogene metamorphic rocks. In contrast, the rocks on the eastern side of the basins are
74 mainly Pliocene–Miocene sedimentary rocks, overlain by unconsolidated alluvial and
75 lacustrine deposits (Matsuta et al., 2001). Geological and seismic reflection data show that
76 the Kamishiro Fault offsets late Pleistocene–Holocene sedimentary strata at an average
77 vertical slip rate of 1.5–3.1 mm/yr (RGAFJ, 1980, 1991; Okumura et al., 1998; Matsuta et al.,
78 2001, 2004, 2007).

79 Historical and instrumental records show that four large earthquakes ($M \geq 5.7$) have
80 occurred close to the active Kamishiro Fault, in the northern vicinity of the Matsumoto Basin,
81 during the past 300 years (Fig. 1b; M 6.3 in 1714; M 5.7 in 1858; M 6.5 and 6.1 in 1918)
82 (Headquarters for Earthquake Research Promotion, 2000). The 1918 M 6.5 Omachi
83 earthquake deformed the ground along a steeply dipping active fault in the Motsumoto Basin

84 (Tada and Hashimoto, 1988). Paleoseismic study reveals that the most recent event on the
85 northern section of the ISTL probably occurred in 841 A.D., indicating a high seismic
86 potential of the ISTL (Okumura et al., 2001). Geologic and seismic reflection data suggest
87 that the active faults that bound the eastern margin of the Matsumoto and Kamishiro basins
88 have the potential to trigger an earthquake of M >8.0 (Headquarters for Earthquake Research
89 Promotion, 2000).

90

91 **3. Co-seismic surface rupture structures**

92 Our field investigations reveal that the 2014 Nagano earthquake produced a 9.3-km-long
93 surface rupture zone, with a combination of thrust and left-lateral strike-slip displacements
94 (Fig. 2). The co-seismic surface ruptures are concentrated within a zone that ranges from a
95 few meters up to 100 m in width, but is generally less than 20 m wide. The surface rupture
96 zone has an irregular curved geometry that largely follows pre-existing fault traces within the
97 Kamishiro Fault zone including a previous unknown active fault (Fig. 2).

98 The co-seismic surface rupture zone is mainly defined by thrust faults, fold structures
99 that include mole tracks and flexural folds, sand boils, and numerous extensional fractures
100 (Figs 3–7). The thrust faults are generally expressed at the ground surface by the discrete
101 fault planes and scarps that characterize much of the co-seismic surface rupture zone (Figs
102 3–7). The principal slip surface was observed at Loc. 2, where Neogene tuff breccia is thrust
103 over alluvial deposits along a fault that dips 30° to the east-southeast (Fig. 3d–f). The total
104 offset amount along the fault plane is estimated to be > 10 m, indicating repeated seismic

105 slipping and accumulation of displacements on the fault after the formation of alluvial
106 deposits. The thrust-dominated slip sense at this locality is recorded by slickenside striations
107 developed on the slip surface (Fig. 3f–g) and by the geometry of fault scarps, which record
108 dominantly vertical movement, with a horizontal slip component (Fig. 3b). Both the surficial
109 deposits and the underlying rock of the mountain slope are folded and offset. At Loc.8, the
110 leaf-covered surface soil of the footwall was overridden by a distance of ~0.4 m by the
111 protruding hanging-wall of the thrust (Fig. 4d). This type of co-seismic thrust fault scarp is
112 known as a "protruded scarp" (Gordon and Lewis, 1980; Lin et al., 2009). Near-surface
113 unconsolidated deposits and surface soil layers were entrained in the protruding
114 hanging-wall of the thrust along the ground surface of the footwall. Similar thrusting and
115 shortening structures have been reported from co-seismic thrust fault scarps worldwide,
116 including the Senya Thrust, which formed during the1896 M 7.5 Rikuu earthquake, northeast
117 Japan (Research Group for the Senya Fault, 1986); the Spitak Thrust, which formed during
118 the 1988 M_s 6.9 Armenian earthquake (Philip et al., 1992); and the co-seismic surface
119 ruptures that occurred within the Longmen–Shan Thrust Belt during the 2008 M_w 7.9
120 Wenchuan earthquake (Lin et al., 2009, 2010). The structural features of the "protruded scarp"
121 suggest that the unconsolidated alluvial deposits in the hanging wall were offset by the fault
122 and slid forward along the fault plane onto the ground surface in the footwall of the fault.

123 At some localities, the co-seismic fault scarps formed along pre-existing fault scarps
124 that record cumulative displacements (Fig. 5). A typical examples was observed at Loc. 6,
125 where a new 1.0-m-high co-seismic fault scarp is superimposed on a 1.0-m-high pre-existing
126 fault scarp that is developed within the alluvial sandy gravel and soil (Fig. 5c). This

127 duplication of surface displacements was also observed at Locs. 14, 16 and 17 along
128 previously-unknown active fault scarps (Fig. 5d-f), indicating that seismic faulting events
129 have occurred repeatedly along the same active fault traces. This new finding shows that the
130 co-seismic surface ruptures not only occurred along the previously-known fault trace of the
131 Kamishiro Fault but also along previously-unknown active faults.

132 Co-seismic folding occurred mainly as flexural folds and mole tracks (Fig. 6). The
133 flexural folds deformed originally horizontal rice fields, which provided a useful marker of
134 the ground surface deformation. The flexural folds include both folding and slip along layer
135 boundaries, as well as some flow within the layers. It is difficult to recognize whether or not
136 slip has occurred along the boundaries of sedimentary layers in active flexural folds, as
137 deformation in weakly consolidated and/or unconsolidated sediments is often not orderly,
138 and outcrops are often not available for observing flexural slip fold structures in the field (Lin
139 et al., 2015a). In this paper we use the term *flexural fold* to describe all varieties of active
140 flexural folds, including flexural flow and flexural slip folds and folds involving the
141 deformation of weakly consolidated and/or unconsolidated sediments. We observed
142 flexural-folds that followed both the NW- and NNE-trending rupture zones, and the
143 deformation is typically distributed across a 2–10-m-wide zone (Fig. 6a–d). Rows of rice
144 plants along the NW-trending flexures were sinistrally offset by 0.2–0.3 m and uplifted up to
145 ~1 m in height (Fig. 6a–b and d), compared with up to 0.5 m of dextral displacement along
146 the NE-trending flexures (Fig. 6c–d). These horizontal displacements reveal evidence of
147 conjugate shearing during the earthquake, which is consistent with an E–W compressional

148 stress in the study area (see Discussion for details). Sinistral displacements also occurred
149 along NNE-trending surface rupture traces as observed at Loc. 2 (Fig. 3b).

150 Mole tracks are widely observed along the co-seismic surface rupture zone. They
151 usually occur within unconsolidated deposits and cemented ground such as roads, where they
152 form a linked array of contractional structures along the rupture zone (Fig. 6e–g). The mole
153 tracks are similar to those produced by the 1999 M_w 7.6 Chi-Chi (Taiwan) earthquake (Lin et
154 al., 2001), the 2001 M_w 7.8 Kunlun earthquake (Lin et al., 2004; Lin and Nishikawa, 2007),
155 the 2008 Wenchuan M_w 7.9 earthquake (Lin et al., 2009, 2010), and the 2010 M_w 6.9 Yushu
156 earthquake (Rao et al., 2011). Mole tracks are a typical contractional structure associated
157 with thrusting and folding (Lin et al., 2004). Numerous sand boils were produced by
158 shaking-induced liquefaction in streams and lowlands, and along the lanes of mole track
159 structures. The sand boils generally occurred as a series of vents aligned parallel to the
160 surface rupture zone (Figs 6g–h and 7a).

161 Extensional cracks and landslides are widely distributed along the surface rupture zone
162 (Fig. 7b–d). Most of extensional cracks occurred in a pattern of left-step en-echelon openings
163 (Fig. 7b–c). A large-scale landslide occurred along a river bank in the co-seismic rupture
164 zone (Fig. 7d).

165

166 **4. Co-seismic displacements**

167 It is generally difficult to obtain field measurements of the amount of co-seismic slip along
168 thrust faults because of the complex geomorphic expression of the co-seismic surface rupture.
169 Difficulties are greatest in areas where the fault plane is not exposed at the surface or where it
170 ruptures through thick deposits of unconsolidated material. We measured the vertical offset
171 displacements at main locations where discrete faults offset ground surface markers such as
172 roads, small gullies, and terrace risers. The latitude and longitude of locations where the
173 structural features of surface ruptures observed and the co-seismic displacements were
174 measured in-site are shown in Table 1. In places where flexural folds result in the
175 deformation of ground surface markers being spread across a 2–30-m-wide zone (generally
176 <10 m), we calculated the vertical displacement by measuring topographical profiles across
177 the scarps and folds using a tape measure and hand level.

178 The slip distribution, based on measured displacements, is shown in Fig. 8 and reveals
179 the dominance of vertical displacements along the entire surface rupture zone. The vertical
180 displacements range from several centimeters to 1.5 m, but are generally in the range 0.4–1.0
181 m. The maximum offset was measured at Loc. 7, where a mountain road is vertically offset
182 by 1.5 m (Fig. 4a). A strike-slip component was also observed at some locations along the
183 surface rupture zone (Fig. 8), with horizontal displacements ranging from 0.1 to 0.6 m. NW-
184 and NNE-trending surface ruptures commonly exhibited a component of left-lateral slip
185 (Figs 6a–b and 8), whereas a right-lateral component of slip was observed at two locations
186 along the NE-trending rupture zone (Figs 6c and 8). The NW-trending surface ruptures with
187 right-lateral offsets can be interpreted as a conjugate structure with the NE-trending fault.
188 The association of dominant vertical displacements and minor, commonly conjugate

189 strike-slip displacements indicates a thrusting mechanism for the earthquake, under an E–W
190 compressive stress.

191

192 **5. Discussion and conclusions**

193 **5.1. Co-seismic surface rupture length and vertical displacement**

194 Offset amount and geometry of co-seismic surface ruptures not only reflects the ground
195 deformation and surface morphology, but also shows the structural characteristics of depth
196 and pre-existing tectonic environment (e.g., Lin et al., 2001, 2009). The co-seismic surface
197 ruptures are restricted to a 9.3-km-long deformation zone that is superimposed on active
198 traces of the Kamishiro Fault, which forms the geomorphic boundary between mountain
199 ranges to the east and basins to the west (Fig. 2). Seismic reflection profiling has shown that
200 the Kamishiro Fault is a thrust fault that consists of several splays distributed across a
201 100–200-m-wide zone (Matsuta et al., 2007). The superimposition of co-seismic
202 displacements on old traces shows that the surface rupturing process, the spatial distribution
203 of surface ruptures, and the co-seismic displacements were all controlled by pre-existing
204 fault structures. Similar observations were made along the thrust faults that produced the
205 1999 M_w 7.6 Chi-Chi earthquake and the 2008 M_w 7.9 Wenchuan earthquake (Lin et al.,
206 2001, 2009).

207 Previous studies have proposed empirical relationships between co-seismic surface
208 rupture length and earthquake magnitude for large intracontinental earthquakes in Japan

209 (Matsuda, 1975, 1998). Matsuda (1998) proposed that surface rupture length (L) is a function
210 of magnitude (M), as follows:

211 $\mathrm{Log}L\ (\mathrm{km}) = 0.72M - 3.92 \qquad 6.8 \leq M \leq 8.0 \qquad (1)$

212 By setting $M = 6.8$, we obtain a rupture length (L) of 9.46 km, which is consistent with our
213 observations.

214 Interferometric Synthetic Aperture Radar (InSAR) data reveal that the total rupture
215 length of the seismogenic fault is ~20 km with a maximum offset of up to ~1 m, is confined to
216 a ~10-km-long rupture zone along the existing trace of the Kamishiro Fault (Fig. 9a). The
217 InSAR analysis show that large offsets of the ground surface occurred along a ~5-km-long
218 section of the southeastern half of the rupture zone (Fig. 9a), which is consistent with our
219 field observations (Figs 8 and 9b). Seismic inversion (Yamanaka, 2014) has shown that i) the
220 seismogenic fault strikes N10°E and dips to the east at 65°, and ii) distinct displacement
221 occurred on a ~15-km-long fault plane. Our field observations confirm that discrete
222 displacement occurred in a 9.3-km-long surface rupture zone, probably caused by
223 propagation of the rupture from the deep source seismogenic fault.

224 NNE-trending fractures with distinct uplift of their east side have also been observed at
225 two locations, ~4–6 km north of our study area, in the northeastern part of the rupture zone
226 (Geospatial Information Authority of Japan, 2014b). If we regard these fractures as
227 co-seismic surface rupture, the total length of the surface rupture zone is increased to ~15 km.
228 Deep snow (>1 m) has so far hindered further field investigations in the epicentral area, and

229 additional work will be required in the spring if we are to better understand the ground
230 deformation characteristics of the seismogenic fault.

231 **5.2. Tectonic implications of co-seismic thrusting and shortening**

232 Documentation and analysis of seismic activity within a fault zone is important for
233 understanding the tectonic behavior of the thrust fault, assessing its mode of crustal
234 deformation, and understanding seismic hazards within the plate boundary zone. The
235 Kamishiro Fault is a major seismogenic component of the ISTL, which forms the plate
236 boundary between the Eurasian and North American Plates, and on which many large
237 historical earthquakes have occurred (Headquarters for Earthquake Research Promotion,
238 2014). We have shown that the geometry and slip distribution of the co-seismic surface trace
239 associated with the 2014 Nagano earthquake, as well as kinematic indicators developed on
240 the main fault plane, all indicate that the co-seismic surface displacement was dominated by
241 thrusting, with a subordinate component of left-lateral slip. This result is consistent with the
242 earthquake focal mechanism (Fig. 1; Yamanaka, 2014). Long-term Global Positioning
243 System (GPS) data (Geospatial Information Authority of Japan, 2014d) have shown that the
244 central part of Honshu Island is currently shortening in a NW-SE to WNW–ESE compressive
245 stress field, which results in the formation of fold–thrust structures. This is consistent with a
246 left-lateral slip component on NNE-trending rupture traces, and right-lateral slip on
247 NW-trending rupture traces (Geospatial Information Authority of Japan, 2014c). It is
248 well-known that the horizontal shortening associated with thrust or reverse faulting could
249 result in apparent shrike-slip movements (apparent horizontal displacements) due to the

250 change in oblique direction between the surface ruptures and displacement markers (Lin et
251 al., 2001). The strike-slip components measured in this study may be partially caused by the
252 geometric orientation of surface ruptures and measured offset markers. Therefore, our
253 findings confirm that the deformation patterns which developed during co-seismic surface
254 rupturing reflect the current compressive environment of the study region.

255 Geological and seismic reflection profiling data indicate an average vertical slip rate of
256 ~1.5–3.1 mma^{-1} for the Kamishiro Fault (RGAFJ, 1980, 1991; Imaizumi et al., 1997;
257 Okumura et al., 1998; Matsuta et al., 2001). Paleoseismic analyses have shown that the
258 recurrence interval of large-magnitude earthquakes for the Kamishiro Fault is ~1100–2340
259 years (Okumura et al., 1998). Our preliminary study reveals that at least three large
260 earthquakes associated with surface rupture of the Kamishiro Fault in the past ~1500 years
261 with an average recurrence interval of ~300-500 years (Lin et al., 2015b). Based on the
262 average slip rate and recurrence interval estimated by our recent study (Lin et al., 2015b),
263 with the typical vertical offsets of 0.4–1 m produced by the Nagano earthquake surface
264 rupture, the vertical slip amount accumulated on the fault during one thousand years is
265 calculated to be ~0.8–3.3 m with an average amount of ~2.0 m. Considering the estimated
266 recurrence interval of large earthquakes, we suggest that large-magnitude earthquakes along
267 the Kamishiro Fault release most of the strain energy that is generated by the current NW–SE
268 compressive stress along the Eurasia–North America plate boundary in the study region. The
269 2014 Nagano earthquake therefore provides an excellent opportunity to study the
270 deformation features within the plate boundary thrust fault zone in the ISTL of northern

271 Honshu Island. Our results show that the Kamishiro Fault plays an important role in crustal
272 deformation and plate boundary strain release within the ISTL active fault zone.

273

274 **6. Conclusions**

275 Based on the results of field investigations conducted following the 2014 Nagano earthquake
276 and above discussion, we arrived at the following conclusions.

277 1.) The 2014 Mj 6.8 (M_w 6.2) Nagano (Japan) earthquake produced a 9.3-km-long
278 co-seismic surface rupture zone.

279 2.) Co-seismic slip occurred on the pre-existing active Kamishiro fault zone, which is
280 dominated by thrusting with subordinate strike-slip displacement.

281 3.) The surface displacements measured in the field range from several centimeters to 1.5 m
282 in the vertical (typically 0.4–1 m), accompanied by a strike-slip component.

283 4.) Our results show that the present-day shortening strain on the Eurasian–North American
284 plate boundary in the study area is released mainly by seismic thrust displacements along
285 the active Kamishiro Fault.

286

287 **Acknowledgements**

288 We thank Dr. M. Tobita of the Geospatial Information Authority of Japan for kind providing

289 the InSAR image data, Profs. M. Hashimoto and K. Okumura for their discussion on the
290 ground deformation caused by the 2014 Nagano earthquake, and Mr. T. Hoshimoto for his
291 kind assistance in the field. We are grateful to two anonymous reviewers for their critical
292 reviews that improved greatly the manuscript. This work was supported by a Science Project
293 grant (Project no. 23253002, awarded to A. Lin) from the Ministry of Education, Culture,
294 Sports, Science and Technology of Japan.
295

296 **References**

297 Geological Society of Japan (eds), 2006. Geology of Japan, Chubu district. Asakura Shoten,
298 Tokyo, Japan, pp.564 (in Japanese).

299 Geospatial Information Authority of Japan, 2012. Maps and geospatial information.
300 http://www.gsi.go.jp/ENGLISH/page_e30031.html (last accessed 20 Dec 2014).

301 Geospatial Information Authority of Japan, 2014a. Information of epicentral area of the
302 Northeren Nagano earthquake.
303 http://www.gsi.go.jp/BOUSAI/h26-nagano-earthquake-index.html (last accessed 20
304 Jan, 2015).

305 Geospatial Information Authority of Japan, 2014b. Investigation on the ground deformation
306 caused by the Northern Nagano earthquake.
307 http://www.gsi.go.jp/cais/topic141203.html (last accessed 20 Jan, 2015).

308 Geospatial Information Authority of Japan, 2014c. Crustal movement of Kantou-Chubu
309 region, central Japan.
310 http://www.gsi.go.jp/WNEW/PRESS-RELEASE/2014-goudou1111.html (last
311 accessed 20 Jan, 2015).

312 Geospatial Information Authority of Japan, 2014d. Crustal movement of Entire Japan.
313 http://cais.gsi.go.jp/YOCHIREN/report/kaihou90/01_04.pdf (last accessed 20 Jan,
314 2015).

315 Gorden, F.R., Lewis, J.D., 1980. The Meckering and Calingiri earthquakes October 1968 and
316 March 1970. Geological Survey of Western Australia Bulletin 126, 1–229.

317 Headquarters for Earthquake Research Promotion, 2000. Evaluation of fault zone geometry
318 of the Itoigawa-Shizuoka Tectonic Line
319 http://www.jishin.go.jp/main/kyoshindo/01a/tenpu1.pdf (last accessed 15 April, 2015*).*
320 Headquarters for Earthquake Research Promotion, 2014. Characteristics of the 2014 Nagano
321 earthquake. http://www.jishin.go.jp/main/yosokuchizu/chubu/p20_nagano.htm (last
322 accessed 15 April, 2015).

323 Imaizumi, T., Haraguchi, T., Nakata (other 8), 1997. Slip rate on the Kamishiro active fault
324 along the northern part of the Itoigawa-Shizuoka Tectonic Line, detected by
325 long-geo-slicer and drilling. Active Fault Research 16, 35–43 (in Japanese with English
326 abstract).
327 Kobayashi, Y., 1983. Initiation of subduction Japan. Geographical Review Japan 50B,
328 49–60.

329 Japan Meteorological Agency, 2014. Earthquake information.
330 http://www.jma.go.jp/en/quake/20141122221109395-222208.html (last accessed 12
331 Jan, 2015). http://www.jma.go.jp/jma/press/1411/23a/201411230000.html (last
332 accessed 15 April, 2015).

333

334 Lin, A., Nishikawa, M., 2011. Shear zone structures of the co-seismic surface ruptures
335 produced by the 2001 M_w7.8 Kunlun earthquake, northern Tibetan Plateau. Journal of
336 Structural Geology 33, 1302–1311.

337 Lin, A., Ouchi, T., Chen, A., Maruyama, T., 2001. Co-seismic displacements, folding and
338 shortening structures along the Chelungpu surface rupture zone occurred during the
339 1999 Chi-Chi (Taiwan) earthquake. Tectonophysics 330, 225–244.

340 Lin, A., Ren, Z., Jia, D., Wu, X., 2009. Co-seismic thrusting rupture and slip distribution
341 produced by the 2008 Mw7.9 Wenchuan earthquake, China. Tectonophysics 471,
342 203–215.

343 Lin, A., Ren, Z., Jia, D., Miyairi, Y., 2010. Evidence for a Tang-Song great earthquake
344 the Longmen Shan Thrust Belt prior to the 2008 M_w7.9 Wenchuan earthquake, China.
345 Journal of Seismology 14, 615–628.

346 Lin, A., Rao, G., Yan, B., 2015a. Flexural-fold structures and Active faults in the
347 northern-western Weihe Graben, central China. *Journal of Asian Earth Sciences*,
348 http://dx.doi.org/10.1016/j.jeaes.2015.04.012, in press.

349 Lin, A., Sano, M., Yan, B., Wang, M., 2015b. Preliminary study of paleoseismicity on the
350 Kamishiro Fault that triggered the 2014 M_w 6.2 Nagano earthquake. Japan Geoscience
351 Union Meeting 2015, Abstract (S-SS28),
352 http://www2.jpgu.org/meeting/2015/PDF2015/index.html (last accessed 22 June
353 2015).

354 Matsuta, N., Ikeda, Y., Imaizumi, T., Sato, H., 2001. Subsurface structure of and rate of the
355 net slip on the Kamishiro fault, northern part of the Itoigawa-Shizuoka tectonic line,
356 central Japan. Active Fault Research 20, 59–70 (in Japanese with English abstract)

357 Matsuta, N., Ikeda, Y., Sato, H., 2004. The slip rate along the northern Itoigawa-Shizuoka
358 tectonic line active fault system, central Japan. Earth Planet. Space 56, 1325–1332.

359 Matsuta, N., Ikeda, Y., Sato, H. et al., 2007. P- and S- wave seismic reflection profiling
360 across the Kamishiro fault, Itoigawa-Shizuoka Tectonic Line active fault system,
361 central Japan. Bulletin of Earthquake Research Institute, University of Tokyo 82,
362 25–35 (in Japanese with English abstract).

363 Matsuda, T., 1975. Magnitude and recurrence interval of earthquake from a fault. Zisin,
364 Journal of Seismological Society of Japan 28, 269–283 (in Japanese with English
365 abstract).

366 Matsuda, T., 1998. Present state of long-term prediction of earthquakes based on active
367 fault data in Japan-an example for the Itoigawa-Shizuoka Tectonic Line Active Fault
368 System. Zisin, Journal of Seismological Society of Japan 50, 23–33 (in Japanese with
369 English abstract).

370 Nakamura, K., 1983. Possibility of a nascent plate boundary at the eastern margin of the
371 Japan Sea. Bulletin of Earthquake Research Institute, University of Tokyo 58,
372 711–722 (in Japanese).

373 Okumura, K., 2001. Paleoseismology of the Itoigawa-Shizuoka tectonic line in central
374 Japan. Journal of Seismology, 5, 411-431.

375 Okumura, K., Imura, R., Imaizumi, T., Togo, M., Sawa, H.,, Mizuno, K., and Kariya, Y.,
376 1998. Recent surface faulting events along the northern part of the Itoigawa-Shizuoka
377 Tectonic Line-Trenching surveys of the Kamishiro Fault and east Matsumoto Basin
378 Faults, ventral Japan. Zisin, the Journal of Seismological Society of Japan 50, 35-51.
379 (in Japanese with English abstract).

380 Philip, H., Rogozhin, E., Cisternas, A., Bousquest, J.C., Borisov, B., Karahanian, A., 1992.
381 The Armenian earthquake of 1988 December 7: faulting and folding, neotectonics and
382 paleoseismicity. Geophysical Journal of International 110, 141-158.

383 Rao, G., Lin, A., Jia, D., Wu, X., Ren, Z., 2011. Co-seismic surface strike-slip shear
384 structures produced by the 2010 M_w6.9 Yushu earthquake, central Tibetan Plateau.
385 Tectonophysics 507, 86-94.

386 Research Group for Active Faults of Japan (RGAFJ), 1980. Active Faults in Japan–Sheet
387 Maps and Inventories. University of Tokyo Press, 363pp (in Japanese with English
388 summary).
389 Research Group for the Senya Fault of Japan (RGAFJ), 1986. Holocene activities and
390 near-surface features of the Senya fault, Akita Prefecture, Japan-excavation study at
391 Komori Senhata-cho. Earthquake Research Institute University of Tokyo Bulletin 61,
392 339–402 (in Japanese with English abstract).

393 Research Group for Active Faults of Japan (RGAFJ) (1991). Active faults in Japan—Sheet
394 maps and inventories (revised edition), Univ. Tokyo Press, Tokyo, 437pp (in Japanese
395 with English summary).
396 Seno, T., Stein, S., Griff, A.E., 1993. A model for the motion of the Philippine Sea plate
397 consistent with NUVEL-1 and geological data. Journal of Geophysical Research 98,
398 17941–17948.

399 Seno, T., Sakurai, T., Stein, S., 1996. Can the Okhotsk plate be discriminated from the
400 North American plate? Journal of Geophysical Research 101, 11305–11315.

401 Yamanaka, Y., 2014. Nov. 22 Northern Nagano earthquake (M6.8). NGY earthquake note,
402 No.55. http://www.seis.nagoya-u.ac.jp/sanchu/Seismo_Note/2014/NGY55.html (Last
403 accessed, 15 April, 2015).

404 Yamazaki, T., Seno, T., 2005. High strain rate zone in central Honshu resulting from the
405 viscosity heterogeneities in the crust and mantle. Earth and Planetary Science
406 Letters 232, 13–27.

Table 1. Main locations of the Nagano co-seismic surface rupture zone, where co-seismic offset amounts were measured in-site.

No	Latitude	Longitude	Altitude (m)	V (m)	H (m)	Surface marker	Figure site
1	137.891647	36.708069	756.89	0.40		Field	Loc. 1
2	137.875812	36.706603	621.11	0.54		Road	
3	137.877864	36.708866	667.98	0.89	L0.28	Path	Loc.2, Fig. 3a-c
4	137.877739	36.708626	669.03	1.18	L0.6	Path	Loc.2, Fig. 7b
5	137.869846	36.697166	696.63	0.39		Field	Loc.5, Fig. 5a
6	137.869977	36.697587	696.54	0.30		Road	
7	137.870547	36.698000	697.6	0.10		Road	
8	137.869617	36.696393	693.23	0.18		Path	
9	137.873103	36.697445	694.78	0.21		Road	
10	137.872216	36.699671	701.35			Road	Loc.3, Figs 5b and 7d,
11	137.872313	36.700793	698.37	0.43		Road	
12	137.868756	36.69132	714.96			Road	Loc.4, Fig. 6f
13	137.870297	36.693930	736.96	0.15		Road	
14	137.878059	36.709145	690.61			Alluvial deposit	Loc.2, Fig. 3d-f
15	137.867529	36.695324	683.93	0.22	L 0.3	Field	
16	137.868382	36.695866	693.35	0.30	L 0.18	Field	
17	137.860459	36.687149	709.39		L 0.14	Road	
18	137.860482	36.687113	706.94	0.08		Field	
19	137.857243	36.651974	740.14			Road	Loc.12
20	137.851594	36.667027	730.75	0.59		Road	Loc.10
21	137.85159	36.667125	733.57	0.34		Road	
22	137.851445	36.667621	729.57			Road	Loc.9, Fig. 6e
23	137.851607	36.66930	726.94	0.19		Field	Loc.9, Fig. 6c
24	137.851499	36.668924	729.4	0.40		Field	
25	137.852163	36.670359	728.57	0.41		Field	Loc.9, Fig. 6d
26	137.852313	36.670722	728.37	0.41		Field	
27	137.85478	36.675045	718.03	0.3~0.5		Road	
28	137.855007	36.675673	718.98	0.08	R0.13	Road	
29	137.856964	36.677620	717.26		R0.03	Road	
30	137.859283	36.679515	706.87	0.19		Road	
31	137.859534	36.679657	705.26		L 0.05~0.07	Road	
32	137.861235	36.680750	712.13	0.35		Ground Surface	
33	137.860959	36.680217	738.02	0.3~0.4		Ground Surface	Loc.8, Fig. 4d
34	137.859342	36.679209	734.62	0.18		Ground Surface	
35	137.859544	36.679175	735.01	0.16		Ground Surface	

36	137.858794	36.679126	729.5	0.27		Ground Surface	
37	137.858679	36.679108	729.61	0.14		Ground Surface	
38	137.858396	36.678844	734.77	0.18		Ground Surface	
39	137.858253	36.678511	732.78	0.10		Ground Surface	
40	137.855695	36.676229	726.38	0.25		Ground Surface	
41	137.861179	36.680408	742.08	0.20	L 0.36	Mountain path	
42	137.861482	36.680311	741.79	0.43		Ground Surface	
43	137.86343	36.681665	800.71	1.54		Mountain path	Loc.7, Fig. 4a
44	137.863566	36.681559	815.74	1.10		Ground Surface	
45	137.863843	36.681081	840	0.25		Ground Surface	
46	137.863744	36.681000	831.35	0.30		Ground Surface	
47	137.863417	36.680824	811.41	0.40		Ground Surface	
48	137.861819	36.680420	746.24	0.35		Ground Surface	
49	137.861862	36.680626	742.1	0.36		Ground Surface	
50	137.861811	36.680978	738.45			Ground Surface	Loc.6, Fig. 5c
51	137.861856	36.680992	736.69	1.00		Ground Surface	
52	137.86165	36.681350	730.96	1.10		Ground Surface	Loc.6, Fig. 4b
53	137.861828	36.681726	728.14	0.95		Ground Surface	Loc.6, Fig. 4c
54	137.863712	36.682486	770.92	0.25		Ground Surface	
55	137.86342	36.681992	765.71	0.20		Ground Surface	
56	137.863215	36.681790	761.78	0.40		Ground Surface	
57	137.862596	36.681372	759.6	0.55		Ground Surface	
58	137.862548	36.681239	759.22	0.10		Ground Surface	
59	137.854315	36.673135	712.59	0.15		Ground Surface	
60	137.852803	36.66182	723.37		L 0.26	Field	Loc.11, Fig. 6a, b
61	137.860706	36.648421	740.75	0.15	L 0.1	Road	
62	137.861688	36.648300	740.51			Road	Loc.14, Fig. 5d
63	137.861882	36.648166	744.18	0.40		Road	
64	137.860112	36.646726	746.22			Field	Loc.14, Fig. 7c
65	137.85222	36.640529	741.74	0.10		Road	
66	137.852292	36.640939	743.35	0.70		Road	
67	137.851469	36.640640	739.86	0.17		Road	Loc.15, Fig. 6g, h
68	137.851539	36.639831	741.95	0.37		Road	
69	137.861	36.650565	756.59			Road	Loc.13, Fig. 7a
70	137.85894	36.651194	756.37	0.08		Road	

No: site number; V: vertical offset; H: Horizontal offset; L: left-lateral component; R: right-lateral component; Loc.1–15: Main locations where the structural features of the co-seismic surface ruptures are shown in Figs 3–7.

Figure1

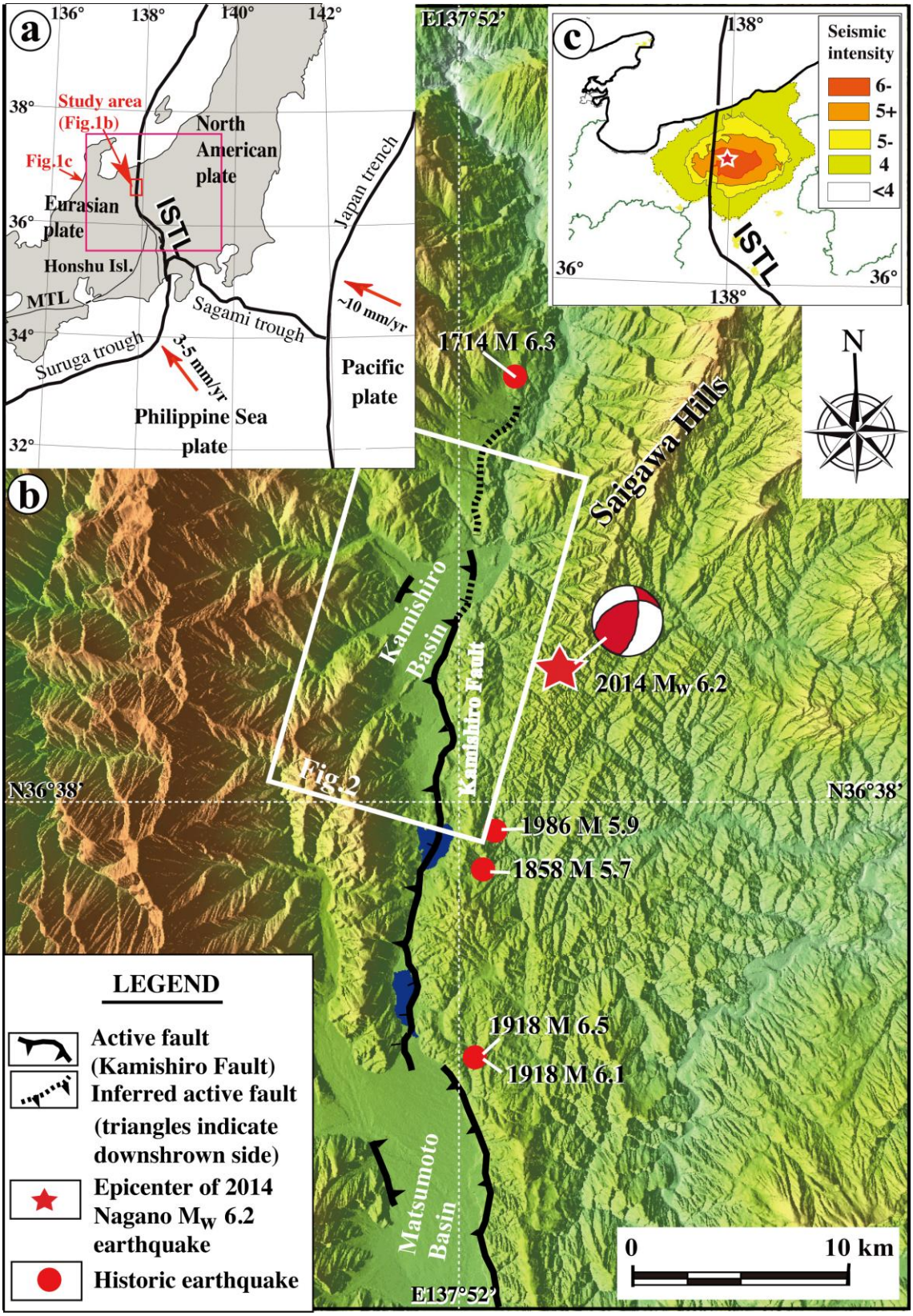

Fig. 1 (a) Index map showing the tectonic setting of the Nagano earthquake. (b)

Color-shaded relief map showing the distribution of active faults in the Matsumoto Basin. Active fault data are from Research Group for Active Faults of Japan [(RGAFJ), (1991)]. Epicenter data are from Geospatial Information Authority of Japan (2014a). Focal mechanism is from Yamanaka (2014). Epicenter data of historic earthquakes (M > 5.7) are from Headquarters for Earthquake Research Promotion (2000). MTL: Median Tectonic Line. ISTL: Itoigawa–Shizuoka Tectonic Line. Honshu Isl.: Honshu Island.

Figure2

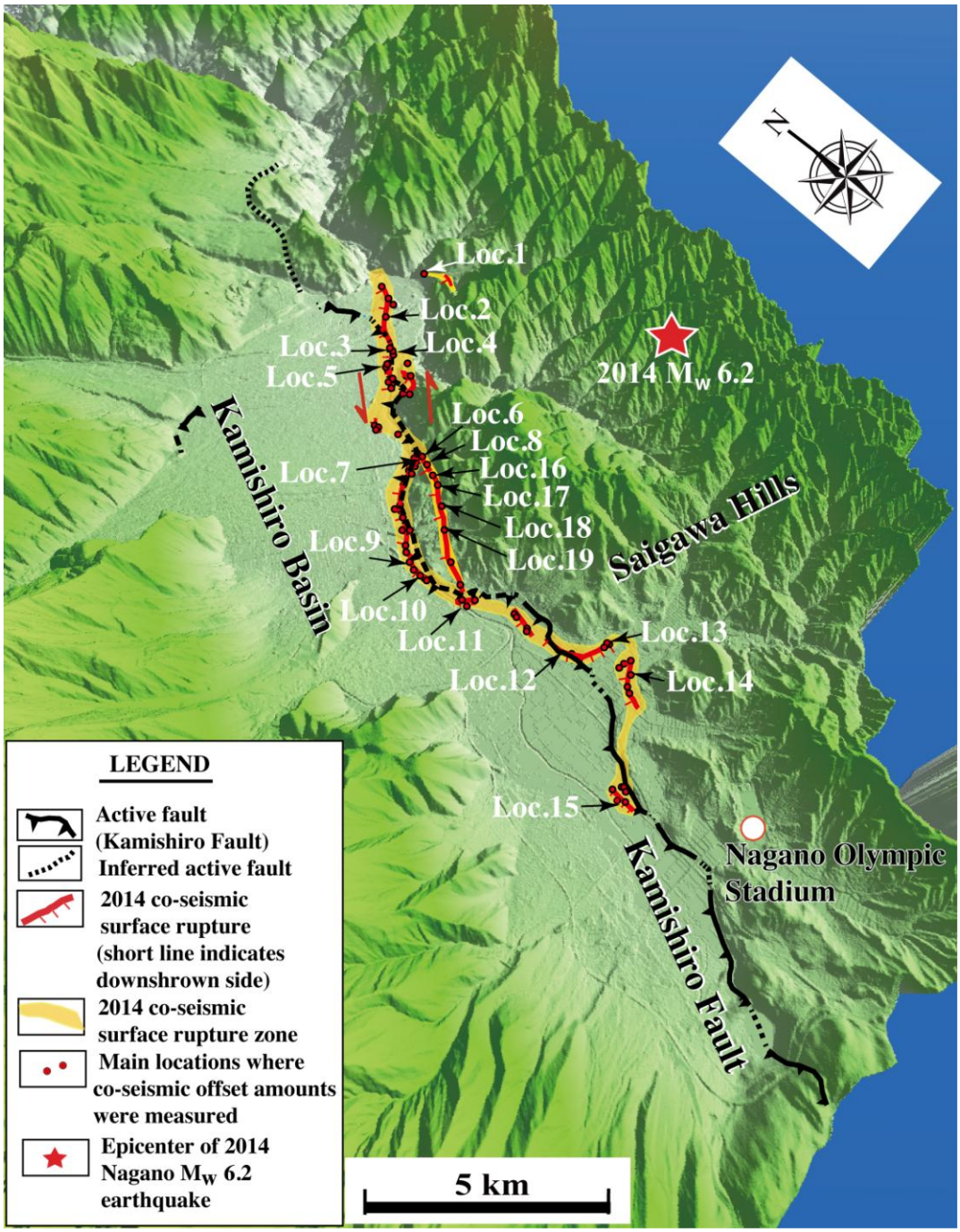

Fig. 2. Color-shaded relief map showing a perspective view of topographic features in the study area, and the distribution of the 2014 Nagano co-seismic surface ruptures. Active fault data are from RGAFJ (1991). For the location, see Fig. 1b.

Figure3

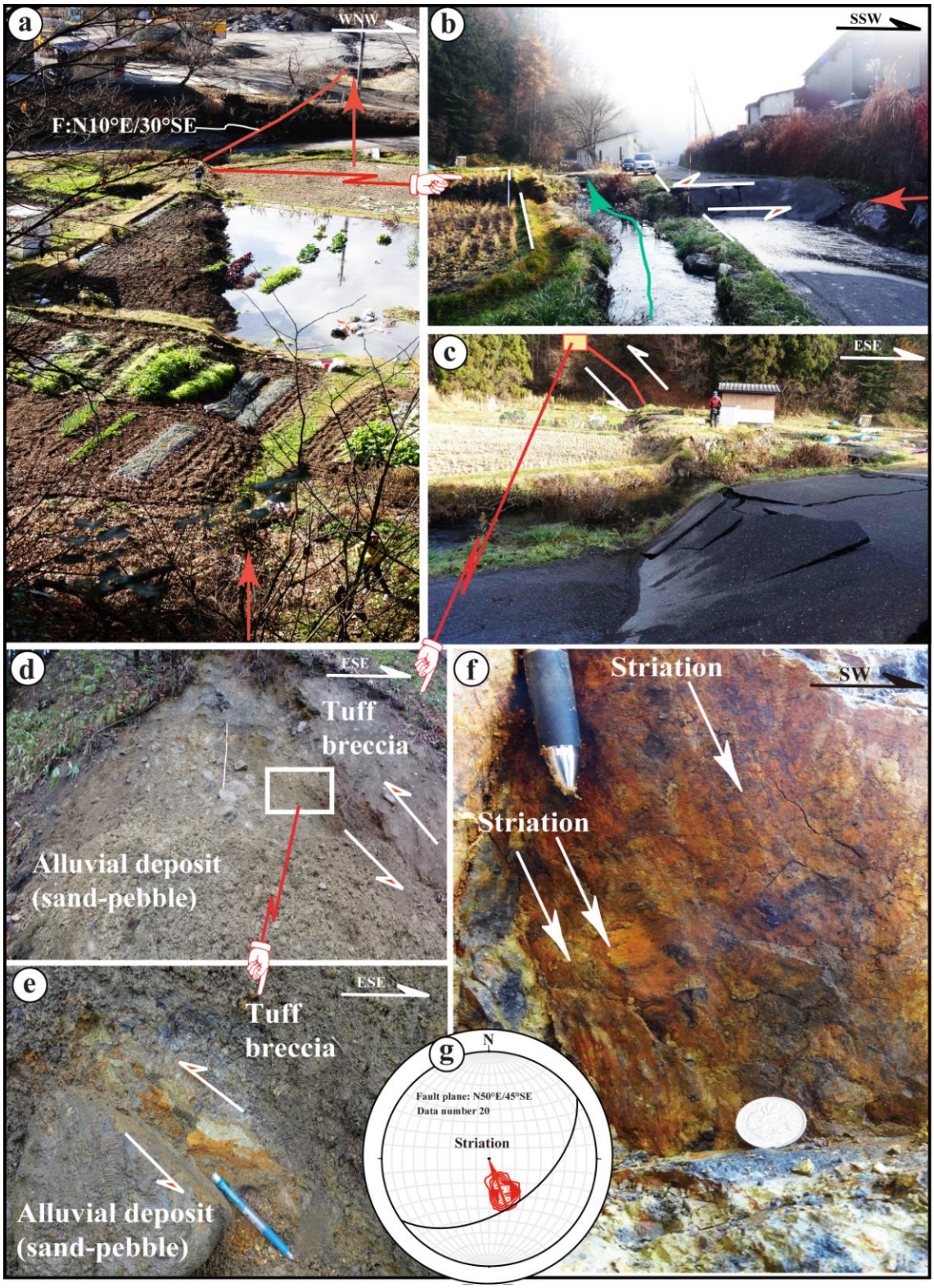

Fig. 3. Representative photographs of co-seismic surface ruptures, showing the thrust

structures associated with the fault scarp at Loc. 2. Red arrows indicate the fault trace. (a) Overview from the NNE of the co-seismic fault scarp. Note that the standing water was dammed on the downthrown side of the fault. (b) Fault scarp viewed from the WSW. White lines indicate the offset edges of the road and farm land. (c) Fault scarp viewed from the SSW, with fault outcrop in background. Red line indicates the fault plane. (d) Detail of the outcrop in (c), showing that co-seismic surface rupture occurred along a fault contact between Neogene tuff breccia and alluvial deposits. (e) Close-up view of (d), showing a foliation developed in the tuff breccia adjacent to the fault plane. The type measure show for scale is 2 m long. (f) Striations on the main fault plane. (g) Stereographic projection showing the orientations of the fault plane and striations shown in (f).

Figure4

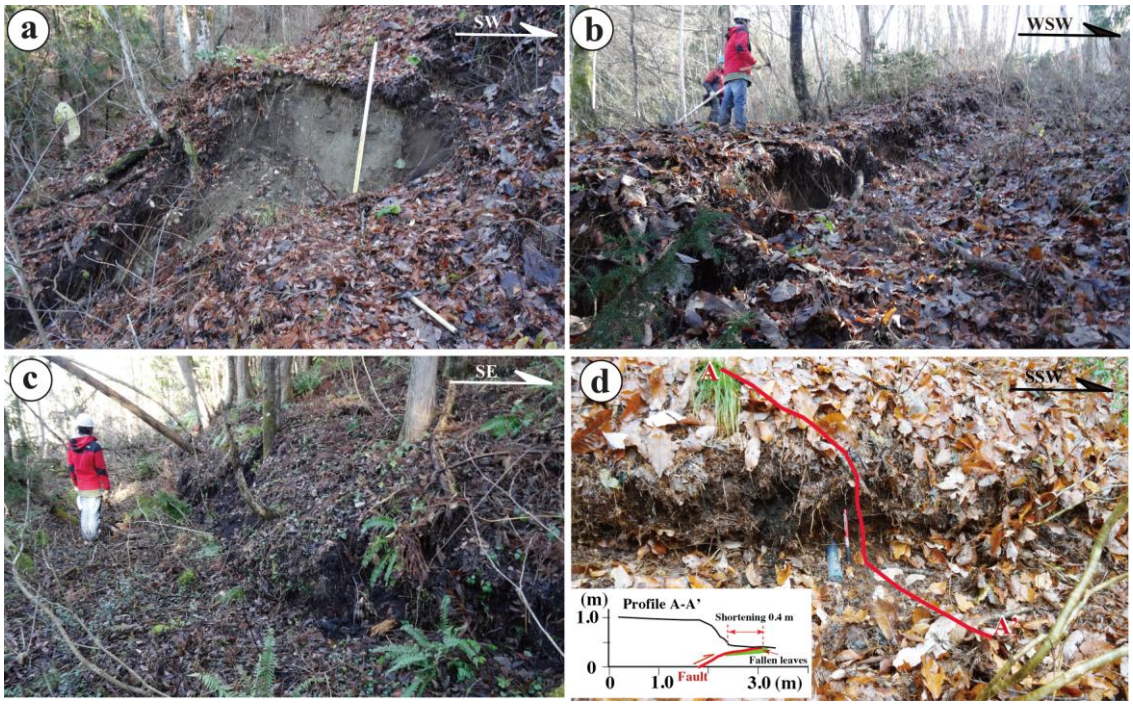

Fig. 4. Representative photographs of co-seismic thrust structures and scarps that developed at Loc. 7 (a), Loc. 6 (b, c) and Loc. 8 (d). (a) The mountain path (on which the hoe was put on) was offset 1.54 m in vertical at Loc. 7. (b) Linear west-facing fault scarp developed on a mountain slope at Loc. 6. (c) Northwest-facing fault scarp observed ~100 m north of Loc. 6. (d) West-facing fault scarp developed on flat ground, at Loc. 8. Note that the ground surface marked by the fallen leaves at the base of the scarp had been horizontally overridden by ~0.4 m, as shown in the topographic profile and cross-section A–A'.

Figure5

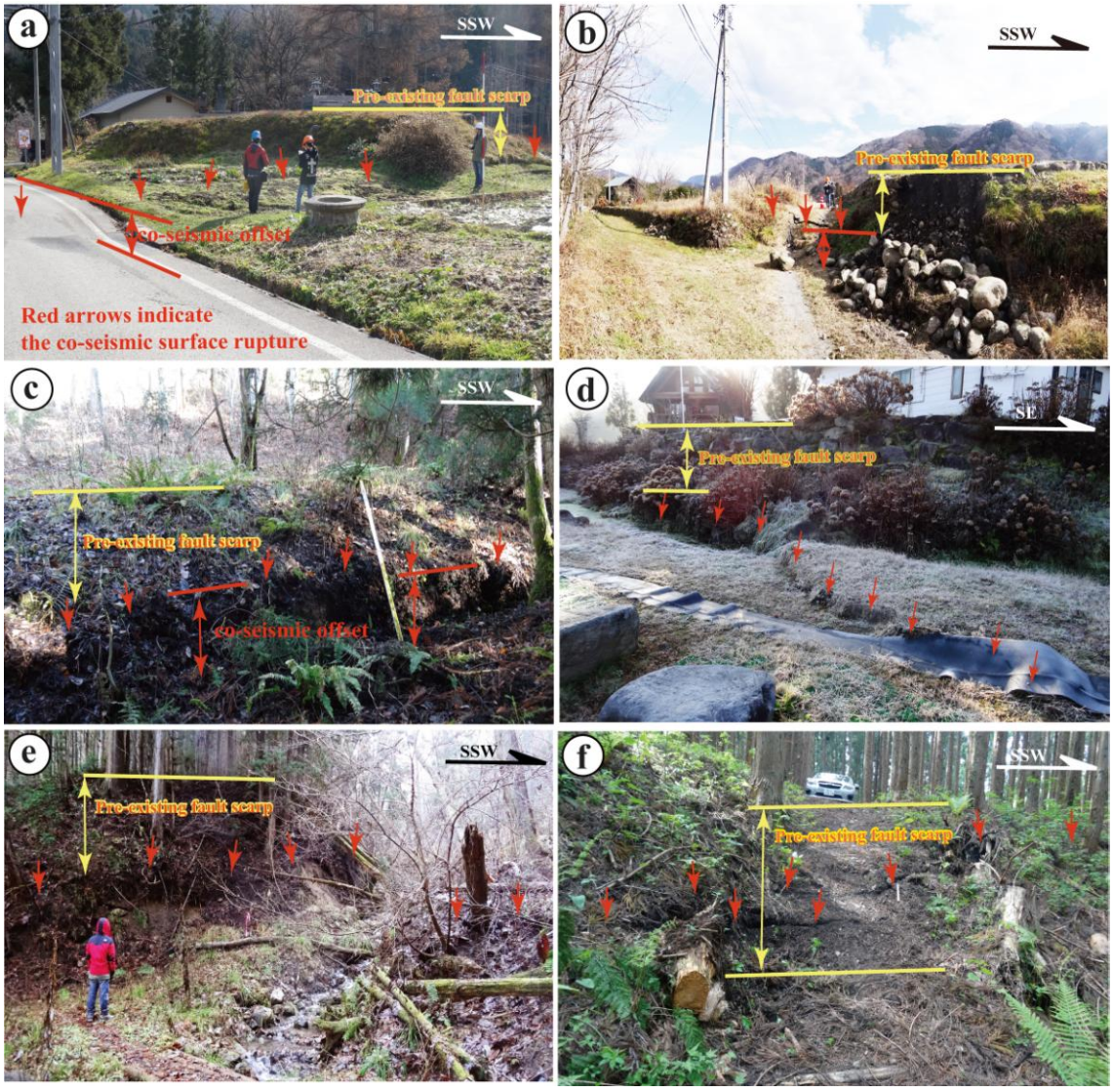

Fig. 5. Representative photographs of co-seismic surface displacements, showing the superimposition of co-seismic flexures and scarps on pre-existing structures. (a) The road and field at Loc. 5 are folded and uplifted to the east by ~0.3 m. The co-seismic surface flexure is superimposed on a 2-m-high pre-existing scarp. (b) A ~0.5-m-high co-seismic scarp at Loc. 3 was superimposed on a pre-existing ~1.5-m-high scarp. (c) A 1-m-high

co-seismic fault scarp duplicated a 1-m-high pre-existing scarp at Loc. 6. (d) At Loc. 14, a 0.3-m-high fault scarp enhanced a pre-existing ~2-m-high fault scarp. (e) A 0.5-high co-seismic fault scarp duplicated a previously-unknown pre-existing scarp at Loc. 16. (f) Co-seismic surfaces duplicated a previously-unknown pre-existing scarp at Loc. 17.

Figure6

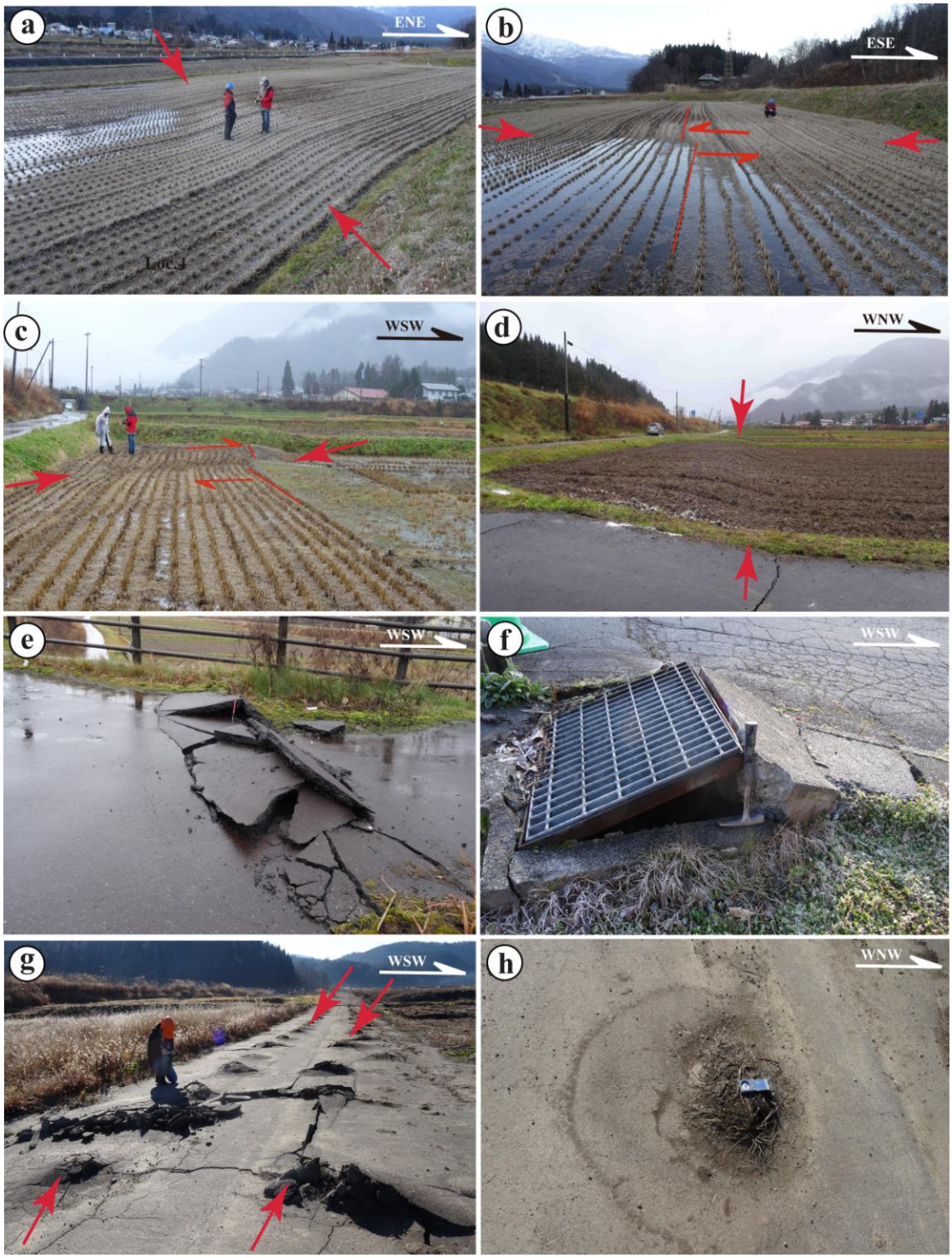

Fig. 6. Representative photographs of co-seismic surface ruptures showing flexural fold structures and liquefaction. (a, b) Sinistral flexural fold developed on a NW-striking fault

trace in a rice field at Loc. 11. The rows of rice plants were offset by ~0.3 m. (c) Dextral flexural folding of rows of rice plants on a N60°E-striking fault trace at Loc. 9. Rice lanes were offset by ~0.35 m. (d) Flexural fold developed on a N15°E-striking fault trace in a rice field at Loc. 9. Note that fault trace shows an irregular orientation from N60°E (shown in c) to N15°E (shown in d). (e, f) Mole track structures developed across a concrete road (e; Loc. 9) and across a ditch (f; Loc. 4). (g) Mole track structures developed in an asphalt road at Loc. 15. The mole tracks form rows along the road within a ~100-m-wide zone. (h) Liquefaction ejected in a mole track structure at Loc. 15.

Figure7

Fig. 7. Representative photographs of co-seismic surface deformation. (a) Differential subsidence caused by liquefaction. The manhole was uplifted by buoyancy forces due to liquefaction at Loc. 13. (b) NE-striking tensional crack at Loc. 2. (c) Tensional cracks in a rice field at Loc. 14. (d, e) Co-seismic surface fractures occurred at Loc. 18 (d) and Loc. 19 (e). (f) NNE-striking tensional cracks over a ~20-m-wide zone developed on the

hanging wall of the fault at Loc. 3 (see Fig. 5b for the details of fault scarp). (g)

Co-seismic landslide in the north end area at a river bank, ~900 m northwest of Loc. 1.

Figure8

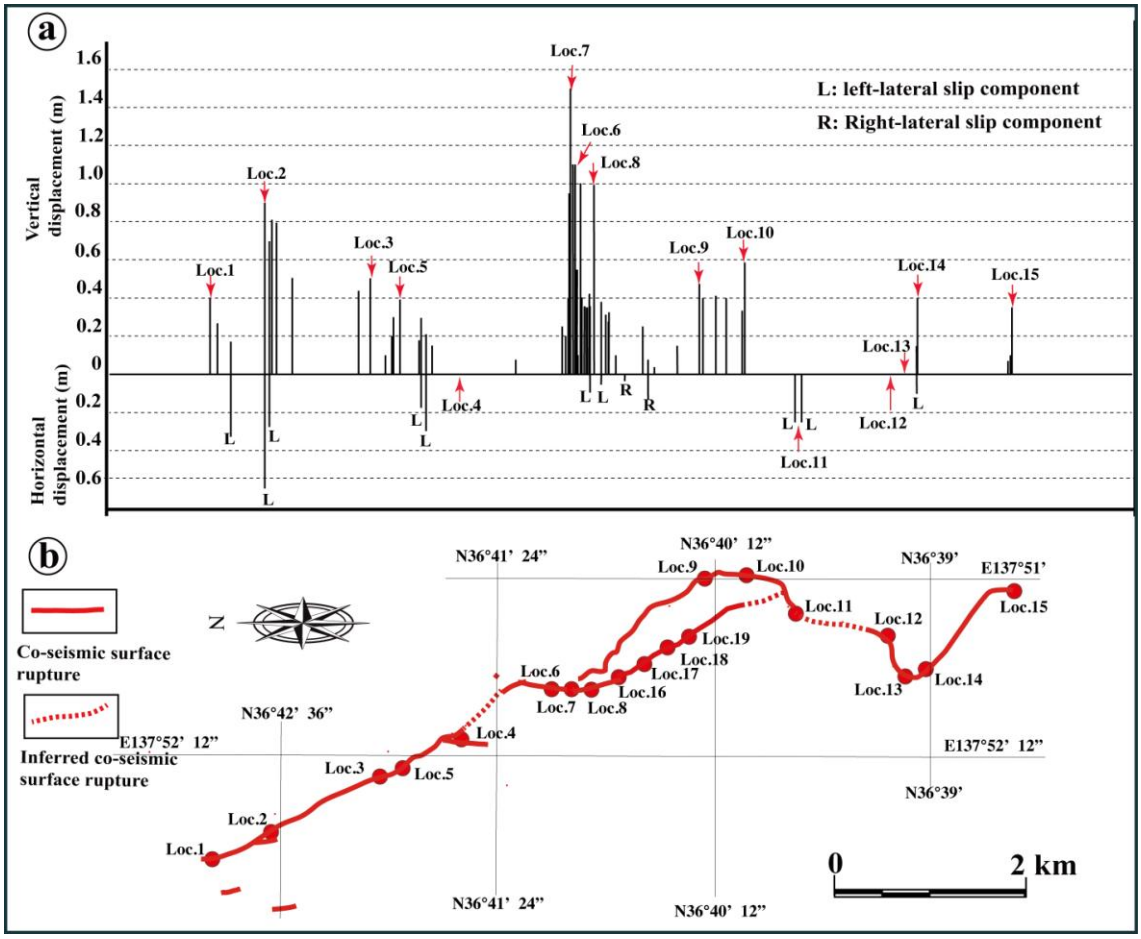

Fig. 8. Slip distribution and rupture trace of the Nagano co-seismic surface rupture zone. (a) Distribution of co-seismic slip, measured along the surface rupture trace. Each measurement was taken at an individual co-seismic surface rupture. The latitude and longitude of the locations where the co-seismic displacements were measured are shown in Table. L: left-lateral slip component; R: right-lateral slip component. (b) Map of the co-seismic surface rupture zone.

Figure9

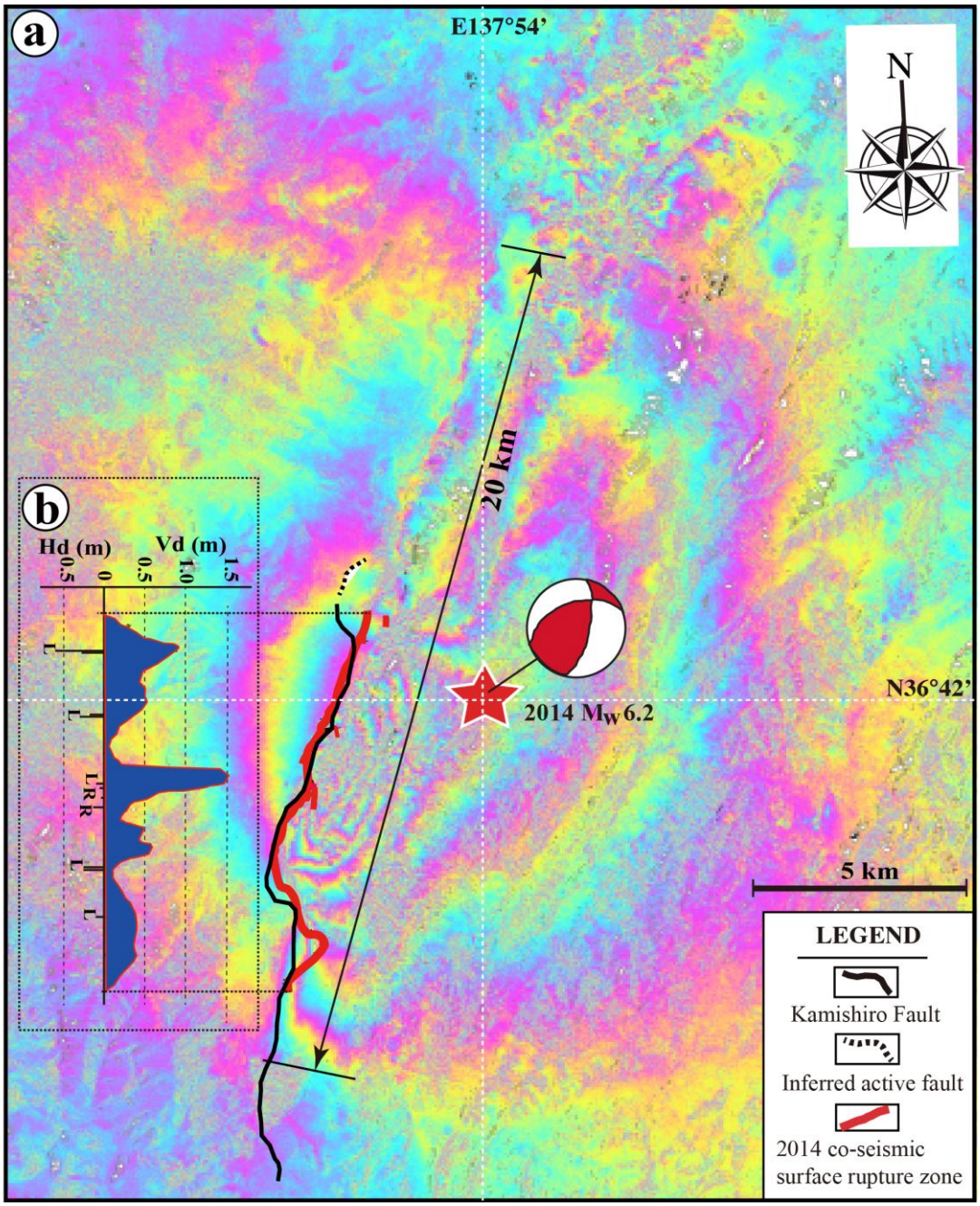

Fig. 9. InSAR interferogram (image provided by the Geospatial Information Authority of Japan) generated from PALSAR-2 data acquired on 2 October 2014 and 27 November 2014. Color fringes are contours of equal ground displacement along the line of sight of

the satellite. One full color cycle represents ~12 cm surface displacement parallel to the line of sight. (a) The co-seismic surface displacement zone was up to 30 km in length. The field-measured offset distribution along the co-seismic surface rupture zone is shown in (b) for comparison. Note that discrete surface ruptures were restricted to a ~10-km-long surface rupture zone in the southwestern segment of the Nagano surface displacement zone.